Supporting information

High strength, high sensitivity integrated wearable signal sensor based on non-covalent interaction of ionic liquid and bacterial cellulose for human behavior monitoring

Table of Contents

Supplementary figures:

Table S1. Composition of the hydrogels.

Figure S1. Diagram of the hydrogel polymerization process.

Figure S2. The zeta potential of BC.

Figure S3. SEM microscopic topography of the ionic sensing hydrogel after freeze-drying

Figure S4. Thermogravimetric analysis of hydrogels with different BC content.

Figure S5. DSC profiles of hydrogels with different [EMIM]Cl additions.

Figure S6. The addition of ionic liquid ([EMIM]Cl) to the mechanical properties of hydrogels.

Figure S7. Dynamic viscoelasticity properties at 25 °C: angular frequency dependence of G′ and G″ ($\omega=10^{-1}$-10^{2} rad/s).

Figure S8. Dynamic viscoelasticity properties at 25 °C: Strain dependence of PAM-BC/[EMIM]Cl_{10} on G 'and G "(ω=1.0 Hz) .

Figure S9. G 'and G "of PAM-BC/[EMIM]Cl_{10} with time (ω = 1.0 Hz; Strain :50%).

Figure S10. Relative resistance at different tensile rates (25-200 mm·min^{-1}) at 200% strain.

Figure S11. Water retention capacity of hydrogels at ~25±2°C and ~60±5% humidity versus water retention time.

Figure S12. Demonstration of the PAM-BC/[EMIM]Cl_{10}-based e-skin applied for typewriting and Depicting pictures by applying PAM-BC/[EMIM]Cl_{10} as a touch screen pen.

Table S2. Comparison of BC-based ion sensing hydrogels in this paper with related sensing gel literature.

Figure S13. Radar chart comparing this paper with related literature.

Supporting Tables and Figures

Composition of the hydrogels. The concentration of BC suspension was measured at 1 wt%. The hydrogel is named PAM-BC/[EMIM]Cl_x in Table S1, where x represents the fraction of the absolute dry mass of BC to the mass of AM.

Table S1. Composition of the hydrogels.

Name (Abbreviation)	AM (g)	[EMIM]Cl (g)	BC(g) 1wt%	MBAA (g)	APS(g)	Water(g)
PAM-BC/[EMIM]Cl_0	4	0.8	0	0.004	0.04	15.16
PAM-BC/[EMIM]Cl_5	4	0.8	2	0.004	0.04	13.16
PAM-BC/[EMIM]$Cl_{7.5}$	4	0.8	3	0.004	0.04	12.16
PAM-BC/[EMIM]Cl_{10}	4	0.8	4	0.004	0.04	11.16
PAM-BC/[EMIM]$Cl_{12.5}$	4	0.8	5	0.004	0.04	10.16
PAM-BC/[EMIM]Cl_{15}	4	0.8	6	0.004	0.04	9.16

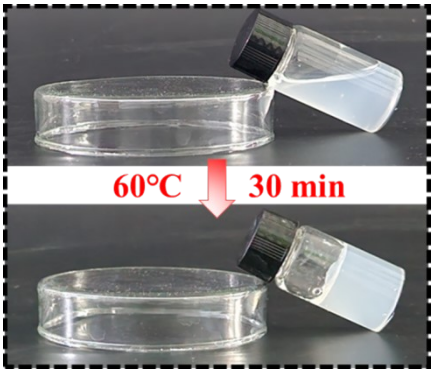

Figure S1. Diagram of the hydrogel polymerization process.

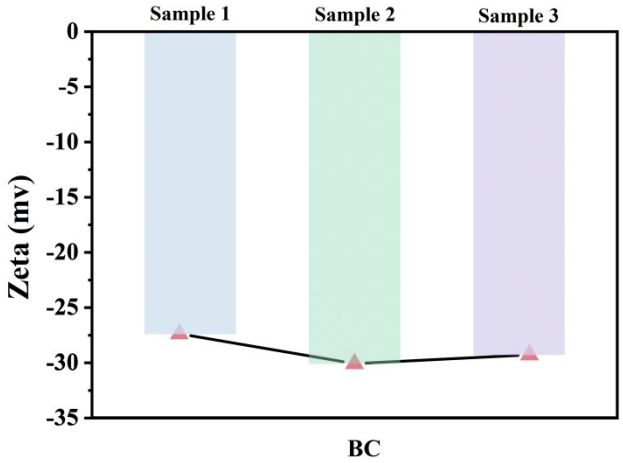

Figure S2. The zeta potential of BC.

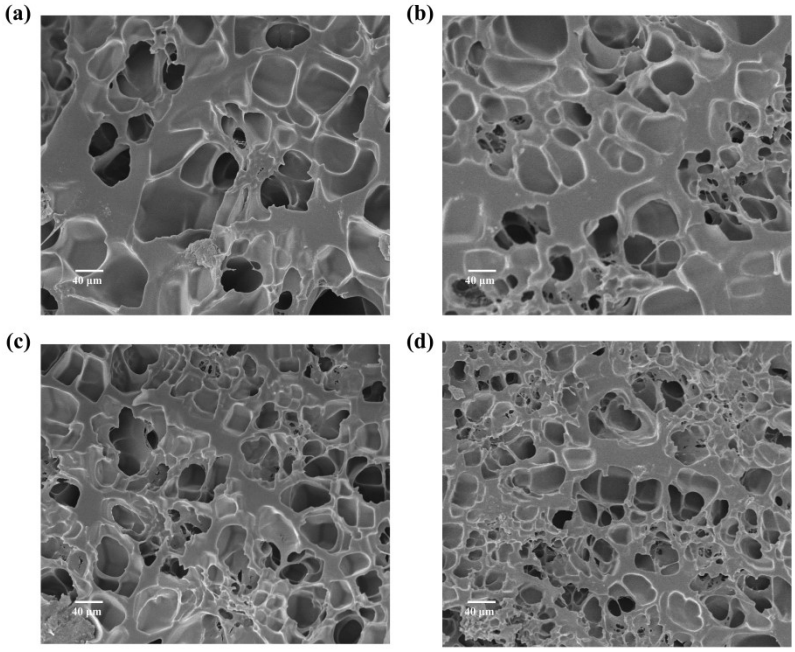

Figure S3. SEM microscopic topography of the ionic sensing hydrogel after freeze-drying

Figure S3a-d show the cross-sectional morphology of lyophilized ion-sensing hydrogels with BC additions of 0 wt‰/7.5 wt‰/10 wt‰/12.5 wt‰ (relative to the weight of AM), respectively. As the proportion of BC in the material increases, the gel network undergoes significant densification. A proper network structure not only increases the mechanical properties of the gel, but also provides pathways for ion migration.

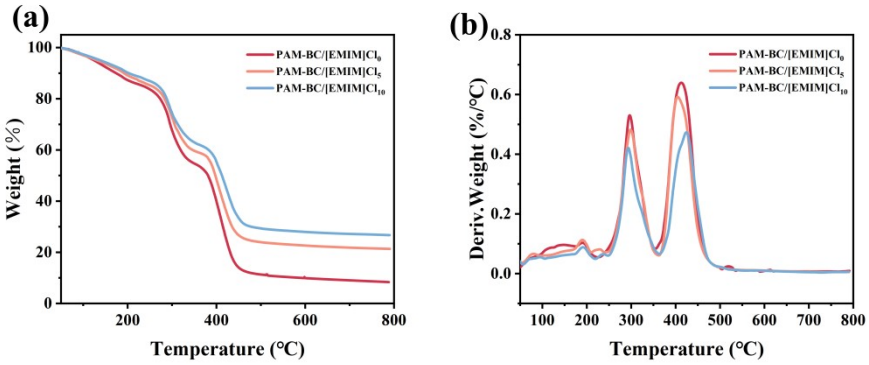

Figure S4. Thermogravimetric analysis of hydrogels with different BC content. (a) Thermogravimetric weight loss profiles for PAM-BC/[EMIM]Cl $_{0/5/10}$. (b) Heat loss rate profiles for PAM-BC/[EMIM]Cl$_{0/5/10}$.

Thermogravimetric experiments were conducted on hydrogels with varying BC contents. Analysis of the thermal weight loss curves and thermal weight loss rate curves depicted in Figure

S4 reveals that the inclusion of BC significantly improves the thermal stability of the hydrogels. This enhancement can be attributed to two primary factors. Firstly, the formation of a three-dimensional network within the gel, facilitated by BC, contributes to the overall improvement in thermal stability. Secondly, the hydroxyl groups in BC exhibit robust water retention properties, effectively slowing down the rate of water loss from the gel.

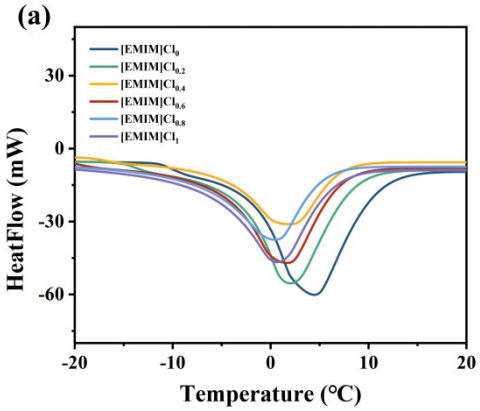

Figure S5. DSC profiles of hydrogels with different [EMIM]Cl additions..

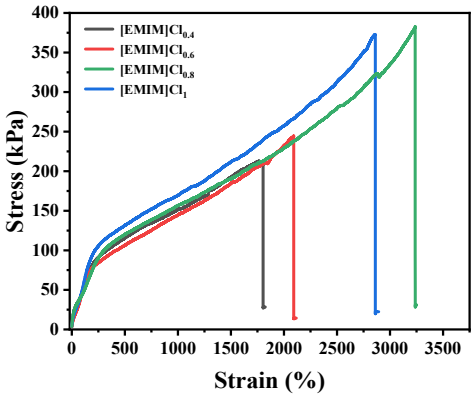

Figure S6. The addition of ionic liquid ([EMIM]Cl) to the mechanical properties of hydrogels.

As shown in Figure S2, the stress-strain images of hydrogels with different [EMIM]Cl additions are shown. The addition amount of BC is fixed at 10‰ of AM, and the amount of [EMIM]Cl is changed to 0.4, 0.6, 0.8, 1 g, respectively. With the increase of ionic liquid, the hydrogen bond and electrostatic interaction sites in hydrogel increased, which significantly

enhanced the mechanical properties of hydrogel. However, the addition of too much ionic liquid increases the stress of the gel and decreases the strain of the hydrogel. As shown in Figure S2, the stress-strain images of hydrogels with different [EMIM]Cl additions are shown. The addition amount of BC is fixed at 10‰ of AM, and the amount of [EMIM]Cl is changed to 0.4,0.6,0.8, 1 g, respectively. With the increase of ionic liquid, the hydrogen bond and electrostatic interaction sites in hydrogel increased, which significantly enhanced the mechanical properties of hydrogel. However, the addition of too much ionic liquid increases the stress of the gel and decreases the strain of the hydrogel.

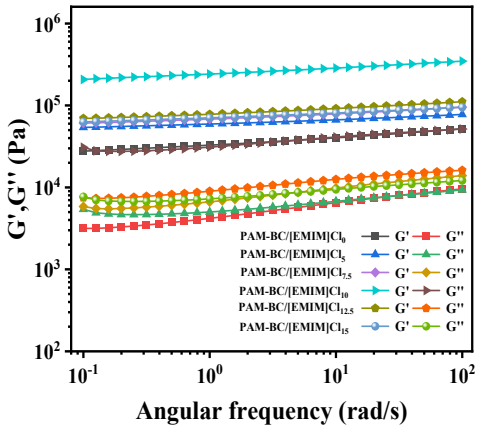

Figure S7. Dynamic viscoelasticity properties at 25 °C: angular frequency dependence of G′ and G″ ($\omega=10^{-1}$-10^{2} rad/s).

The viscoelastic properties of the hydrogel are shown in Figure S3. Changes of dynamic storage modulus G 'and loss modulus G "for hydrogels with different BC content in the frequency range of 10^{-1}-10^{2} rad/s. As expected due to the increased degree of interpenetration and non-covalent crosslinking of BC and [EMIM]Cl in the polymer network, G 'and G' significantly increased with the increase of BC over the frequency range. In the frequency range, the G "of all hydrogels is much higher than G", which is consistent with the solid elastic properties of hydrogels. PAM-

BC/[EMIM]Cl_{10} had the highest G 'and G'.

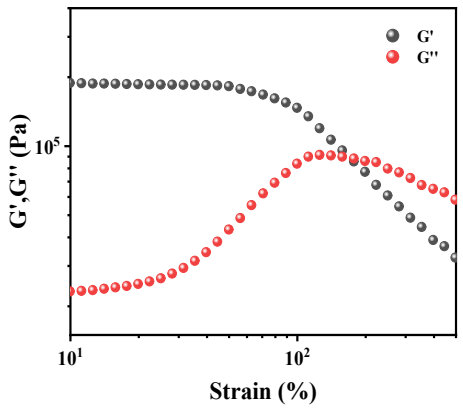

Figure S8. G 'and G "of PAM-BC/[EMIM]Cl_{10} with strain dependence (ω = 1.0 Hz).

PAM-BC/[EMIM]Cl_{10} was selected as the sample for strain scanning measurement. In the < 100% linear viscoelastic region, the G "of the hydrogel is always greater than G". Under large shear strain (> 100%), the hydrogel exhibited nonlinear viscoelastic behavior. G "and G" cross, which was due to the breakdown of the internal network of the hydrogel. The intersection strain of PAM-BC/[EMIM]Cl_{10} was appeared at 109.1%. The addition of BC makes the hydrogel not easy to be induced by shear force and strain, resulting in large-scale deformation of the network structure and unentanglement of crosslinking points, thus obtaining superior mechanical properties. The above results are consistent with those of tensile test.

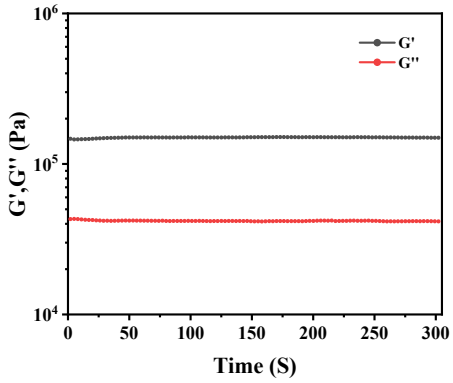

Figure S9. G 'and G "of PAM-BC/[EMIM]Cl_{10} with time (ω = 1.0 Hz; Strain :50%).

Figure S5 shows the excellent stability of PAM-BC/[EMIM]Cl_{10} hydrogel. Thanks to the stability of the internal network of the hydrogel, G "and G" did not change significantly during the rheological test for 5 min.

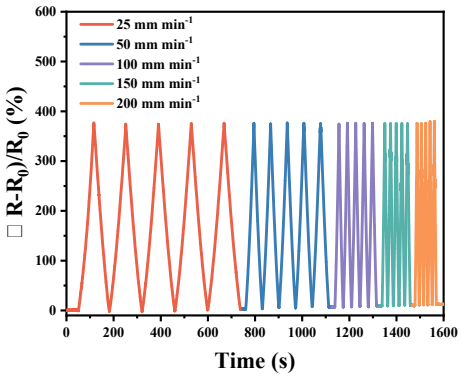

Figure S10. Relative resistance at different tensile rates (25-200 mm·min^{-1}) at 200% strain.

Figure S6 shows the $(R-R_0)/R_0$ values of PAM-BC/[EMIM]Cl_{10} hydrogel under 200% strain at different tensile speeds. The $(R-R_0)/R_0$ values at different stretching speeds (25-200 mm·min−1) did not change significantly, indicating that the sensing properties of hydrogel stability were not affected by the stretching speed.

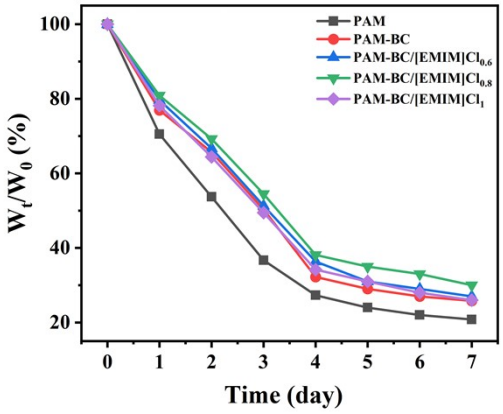

Figure S11. Water retention capacity of hydrogels at ~25±2° C and ~60±5% humidity versus water retention time.

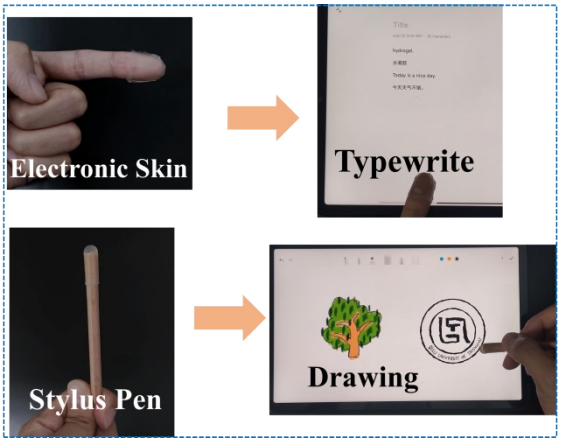

Figure S12. Demonstration of the PAM-BC/[EMIM]Cl_{10}-based e-skin applied for typewriting and Depicting pictures by applying PAM-BC/[EMIM]Cl_{10} as a touch screen pen.

Table S2. Comparison of BC-based ion sensing hydrogels in this paper with related sensing gel literature.[1-10]

Gel Conductors	Stress (kPa)	Strain (%)	Conductivity (mS cm^{-1})	Label name	Reference
PAM-BC/[EMIM]Cl	385.1	3271	2.23		This work
MXene/PHMP	110	680	0.15	He	[1]
PNAGA-NP	728	436	0.26	Zhang	[2]
PGMS	95	2600	8.5	Ma	[3]
SAIFs	1550	161	2.29	Tong	[4]
3A-ADSP-LiCl	399	770	2.9	Wang	[5]
OGTCG	152	225	2.3	Cui	[6]
PNAGA/PNIPAm/AgNW	350	1800	—	Ge	[7]
CNF/ PEDOT:PSS/PAM	240	1881	—	Wang	[8]
OH-PAM-PB-PPy	50	510	1.2	Bei	[9]
PAA/PANI	120	2830	1.4	Liu	[10]

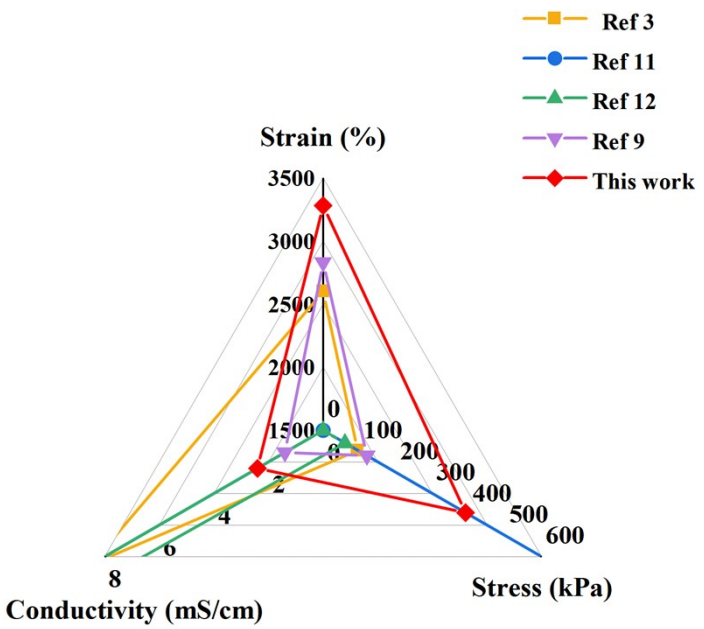

Figure S13. Radar chart comparing this paper with related literature.[3, 9, 11, 12]

References

[1] S. He, B. Guo, X. Sun, M. Shi, H. Zhang, F. Yao, H. Sun, J. Li, Bio-Inspired Instant Underwater Adhesive Hydrogel Sensors, ACS Applied Materials & Interfaces 14(40) (2022) 45869-45879.

[2] Y. Zhang, H. Lu, M. Li, B. Yan, R. Ran, Near-Infrared Laser "Weldable" Hydrogen-Bonded Hydrogel Sensor Based on Photothermal Gel–Sol Transition, ACS Sustainable Chemistry & Engineering 9(48) (2021) 16241-16250.

[3] Y. Ma, D. Zhang, Z. Wang, H. Zhang, H. Xia, R. Mao, H. Cai, H. Luan, Self-Adhesive, Anti-Freezing MXene-Based Hydrogel Strain Sensor for Motion Monitoring and Handwriting Recognition with Deep Learning, ACS Applied Materials & Interfaces (2023).

[4] R. Tong, Z. Ma, P. Gu, R. Yao, T. Li, M. Zeng, F. Guo, L. Liu, J. Xu, Stretchable and sensitive sodium alginate ionic hydrogel fibers for flexible strain sensors, International Journal of Biological Macromolecules 246 (2023) 125683.

[5] Y. Wang, L. Song, Q. Wang, L. Wang, S. Li, H. Du, C. Wang, Y. Wang, P. Xue, W.-C. Nie, Multifunctional acetylated distarch phosphate based conducting hydrogel with high stretchability, ultralow hysteresis and fast response for wearable strain sensors, Carbohydrate Polymers (2023) 121106.

[6] S. Cui, S. Zhang, F. Zhang, R. Lin, C. Tang, X. Jing, Tannic acid-coated cellulose nanocrystal-reinforced transparent multifunctional hydrogels with UV-filtering for wearable flexible sensors, Carbohydrate Polymers (2023) 121385.

[7] S.J. Ge, S.N. Liu, Z.Z. Gu, H. Xu, A Skin-Inspired Multifunctional Conductive Hydrogel with High Stretchable, Adhesive, Healable, and Decomposable Properties for Highly Sensitive Dual-Sensing of Temperature and Strain, Small Methods (2023) 2300749.

[8] Y. Wang, S. Zeng, S. Shi, Y. Jiang, Z. Du, B. Wang, X. Li, Hybrid assembly of conducting nanofiber network for ultra-stretchable and highly sensitive conductive hydrogels, Journal of Materials Science & Technology 169 (2024) 1-10.

[9] Z. Bei, Y. Chen, S. Li, Z. Zhu, J. Xiong, R. He, C. Zhu, Y. Cao, Z. Qian, A self-adhesive and low-temperature-tolerant strain sensor based on organohydrogel for extreme ice and snow motion monitoring, Chemical Engineering Journal 451 (2023) 138675.

[10] D. Liu, H. Zhou, Y. Zhao, C. Huyan, Z. Wang, H. Torun, Z. Guo, S. Dai, B.B. Xu, F. Chen, A Strand Entangled Supramolecular PANI/PAA Hydrogel Enabled Ultra-Stretchable Strain Sensor, Small 18(47) (2022) 2203258.

[11] X. Pan, Q. Wang, R. Guo, Y. Ni, K. Liu, X. Ouyang, L. Chen, L. Huang, S. Cao, M. Xie, An integrated transparent, UV-filtering organohydrogel sensor via molecular-level ion conductive channels, Journal of Materials Chemistry A 7(9) (2019) 4525-4535.

[12] Q. Wang, X. Pan, C. Lin, D. Lin, Y. Ni, L. Chen, L. Huang, S. Cao, X. Ma, Biocompatible, self-wrinkled, antifreezing and stretchable hydrogel-based wearable sensor with PEDOT: sulfonated lignin as conductive materials, Chemical Engineering Journal 370 (2019) 1039-1047.